NUCL SCI TECH (2017) 28:135
DOI 10.1007/s41365-017-0285-9

Evaluation of the fraction of delayed photoneutrons for TMSR-SF1

Rui-Min Ji[1,2] · Ye Dai[1] · Gui-Feng Zhu[1] · Shi-He Yu[1] · Yang Zou[1] · Gui-Min Liu[1]

Received: 19 September 2016 / Revised: 24 December 2016 / Accepted: 30 December 2016 / Published online: 21 August 2017

Abstract The 10 MW_{th} solid-fueled thorium molten salt reactor (TMSR-SF1) is a FLiBe salt-cooled pebble bed reactor to be deployed in 5–10 years, designed by the TMSR group. Due to a large amount of beryllium in the core, the photoneutrons are produced via (γ, n) reactions. Some of them are generated a long time after the fission event and therefore are considered as delayed neutrons. In this paper, we redefine the effective delayed neutrons into two fractions: the delayed fission neutron fraction and the delayed photoneutron fraction. With some reasonable assumptions, the inner product method and the *k*-ratio method are adopted for studying the effective delayed photoneutron fraction. In the *k*-ratio method, the Monte Carlo code MCNP6 is used to evaluate the effective photoneutron fraction as the ratio between the multiplication factors with and without contribution of the delayed neutrons and photoneutrons. In the inner product method, with the Monte Carlo and deterministic codes together, we use the adjoint neutron flux as a weighting function for the neutrons and photoneutrons generated in the core. Results of the two methods agree well with each other, but the *k*-ratio method requires much more computing time for the same precision.

Keywords Photoneutron · Effective delayed neutron fraction · TMSR-SF1

1 Introduction

Fluoride salt-cooled high-temperature reactor (FHR) is a new reactor concept that has gained great attention worldwide [1, 2]. Different from the gas cooled reactors, the liquid salt enables operation with higher power density and provides higher heat capacity. With unique features, an FHR contains technologies derived from earlier reactor designs [3]. In recent years, the thorium molten salt reactor (TMSR) group of Chinese Academy of Sciences (CAS) proposed the 10 MW_{th} solid-fueled TMSR (TMSR-SF1) as China's first FHR to be deployed in 5–10 years [4–6]. In the design, TMSR-SF1 uses coated particle fuel and the beryllium-based salt FLiBe ($^7Li_2BeF_4$) as its primary coolant.

Since there is a large amount of beryllium in the core, photoneutrons are generated via (γ, n) reaction. This reaction requests the threshold energy of 1.67 MeV for the photons. In general, the photoneutrons have little contribution to the overall neutron balance. However, like the delayed fission neutrons which are generated from a few milliseconds to a few minutes after the fission event, some photoneutrons are generated from a few minutes to a few days after the fission event. Thus, the photoneutrons are considered as delayed neutrons. Since they have an insignificant contribution and the equilibrium state is difficult to reach, some researchers omitted the photoneutrons

This work was supported by the Chinese TMSR Strategic Pioneer Science and Technology Project (No. XDA02010000).

✉ Yang Zou
zouyang@sinap.ac.cn

✉ Gui-Min Liu
liuguimin@sinap.ac.cn

[1] Shanghai Institute of Applied Physics, Chinese Academy of Sciences, Jiading Campus, Shanghai 201800, China

[2] University of Chinese Academy of Sciences, Beijing 100049, China

in experimental analysis. Therefore, there are measurement errors caused by neglecting the photoneutrons [7–12]. In the LITR reactor, which uses beryllium reflectors, it was found that the control rod worth would be underestimated for about 6% if neglecting the photoneutrons in the rod-drop measurement [10]. In VVRSZM type research reactor of KFKI-AEKI [8], which uses beryllium reflectors, the reactivity meter gave false values without taking into account the photoneutrons. In the miniature neutron source reactor using beryllium reflectors, the reactivity meter gave greater values by considering the photoneutrons. [11]

Considering that the photoneutrons may impact certain dynamic characteristics, in this paper we focus on evaluating the effect of photoneutrons on β_{eff} for the TMSR-SF1. This paper is organized as follows. Section 2 briefly introduces TMSR-SF1 reactor. Section 3 presents the description of the methodology and the codes used. Section 4 presents results and analyses. Finally, the conclusions are presented in Sect. 5.

2 TMSR-SF1 core configurations

The pebbles in the TMSR-SF1 are 6 cm in diameter. Tri-structural isotropic (TRISO) particles are made up of 17.0% enriched UO_2 kernels coated with a low-density buffer layer, an inner pyrolytic carbon (iPyC) layer, an intermediate silicon carbide (SiC) layer and an outer pyrolytic carbon (oPyC) layer. Parameters of the fuel element are listed in Table 1. A schematic representation of the TMSR-SF1 reactor is shown in Fig. 1. The TMSR-SF1 configuration consists of an active zone, a reflector zone and the vessel. The active zone includes a cylinder and two circular truncated cones. The radius of the cylinder is sized at Φ 135 cm $\times$ 180 cm. The circular truncated cones are sized at Φ 135 cm $\times$ 30 cm. In the active zone, the fuel pebbles are randomly distributed and the coolant is circulating through the pebbles. Thickness of the upper and lower reflectors is 30 cm in minimum. The side reflector is 75 cm thick. In the reflector zone, the graphite blocks host the control rods, neutron detectors, temperature detectors, etc. To protect the control rods and detectors from FLiBe, Hastelloy N alloy tubes are used in the channels. The nominal temperatures of pebble kernel, layers, matrix, shell, FLiBe coolant and reflector graphite are 1050, 1000,

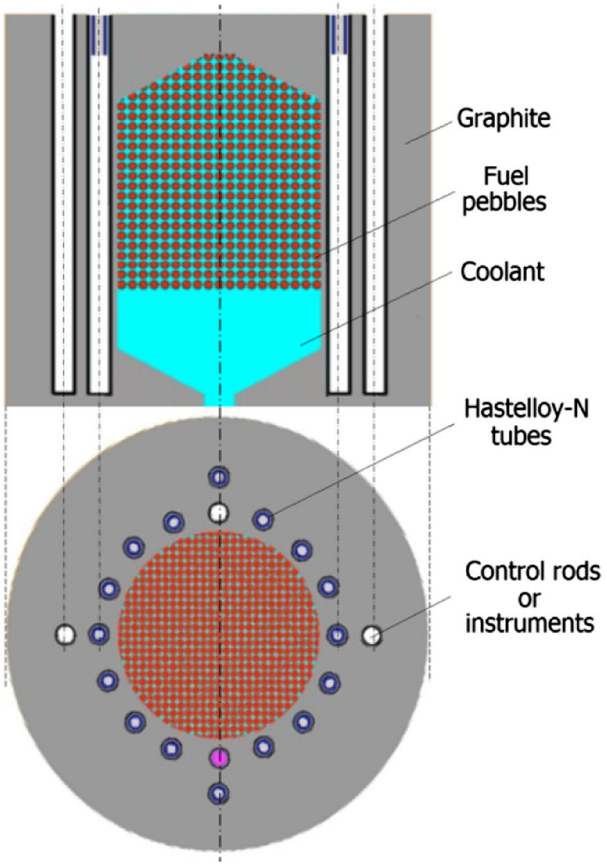

Fig. 1 (Color online) TMSR-SF1 model

Table 1 TMSR-SF1 fuel element characteristic parameters

Parameters	Values
Pebble diameter (cm)	6.0
Fuel zone diameter (cm)	5.0
U loading per pebble (g)	7.0
^{235}U enrichment (%)	17
Equivalent boron content in fuel (ppm)	4
Graphite density (g/cm^3)	1.73
Equivalent boron content in graphite (ppm)	3
Fuel kernel radius (mm)	0.25
UO_2 density (g/cm^3)	10.4
Coating materials	Buffer/iPyC/SiC/oPyC
Layer thickness (mm)	0.095/0.040/0.035/0.040
Layer densities (g/cm^3)	1.10/1.90/3.18/1.90

980, 940, 900 and 880 K, respectively. The FLiBe density is 1.97 g/cm^3 and Li-7 enrichment is 99.99%. The reflector density is 1.825 g/cm^3.

3 Methods

3.1 Theoretical analysis

The time-dependent transport equation for a system without external source can be written as [13]

$$\mathbf{L}\boldsymbol{\Phi} = \omega\mathbf{G}\boldsymbol{\Phi}, \tag{1}$$

where $\boldsymbol{\Phi}$ is a vector including the neutron flux (φ) and photon flux (ψ), $\mathbf{L}$ is the loss operator, $\mathbf{G}$ is the generation operator and $\omega = 1/k$ is the inverse of the classical multiplication eigenvalue. It can be further written as follows

$$\boldsymbol{\Phi} = \begin{pmatrix} \phi \\ \psi \end{pmatrix}, \tag{2}$$

$$\mathbf{L} = \begin{pmatrix} \mathbf{M}^{\mathrm{n}} & 0 \\ 0 & \mathbf{M}^{\gamma} + \mathbf{H}^{\mathrm{ph}} \end{pmatrix}, \tag{3}$$

$$\mathbf{G} = \begin{pmatrix} \mathbf{F}_{\mathrm{p}}^{\mathrm{n}} + \mathbf{D}_{\mathrm{d}}^{\mathrm{n}} & \mathbf{H}^{\mathrm{ph}} \\ \mathbf{F}_{\mathrm{p}}^{\gamma} + \mathbf{D}_{\mathrm{d}}^{\gamma} & 0 \end{pmatrix}, \tag{4}$$

where $\mathbf{M}$ is the removal operator; and the superscripts n and γ denote neutronic and photonic operators or functions, respectively. So, $\mathbf{M}^{\mathrm{n}}$ is the neutron operator and $\mathbf{M}^{\gamma}$ is the photon removal operator. For a system containing Be, neutrons are generated from fissions ($\mathbf{F}^{\mathrm{n}}$) and (γ, n) reactions ($\mathbf{H}^{\mathrm{ph}}$). The $\mathbf{F}^{\mathrm{n}}$ includes a prompt term ($\mathbf{F}_{\mathrm{p}}^{\mathrm{n}}$) and a delayed term ($\mathbf{D}_{\mathrm{d}}^{\mathrm{n}}$). $\mathbf{H}^{\mathrm{ph}}$, which describes the neutrons produced by Be(γ, n) reaction, includes a prompt term ($\mathbf{H}_{\mathrm{p}}^{\mathrm{ph}}$) and a delayed term ($\mathbf{H}_{\mathrm{d}}^{\mathrm{ph}}$) according to the photon source. The photons are generated directly after the fission events ($\mathbf{F}_{\mathrm{p}}^{\gamma}$) or from the decay of the precursors ($\mathbf{D}_{\mathrm{d}}^{\gamma}$). Definitions of the operators are listed in Table 2, which are fairly conventional, but some terms deserve further clarifications. $\chi_{\mathrm{p},m}^{\mathrm{n}}$ and $\chi_{\mathrm{d},m}^{\mathrm{n}}$ are prompt and delayed neutron spectra for fissionable nuclide m, respectively. $\nu_{\mathrm{p},m}^{\mathrm{n}}$ and $\nu_{\mathrm{d},m}^{\mathrm{n}}$ are the prompt and delayed neutron yields per fission for nuclide m, respectively. $\Sigma_{\mathrm{f},m}$ and $\sigma_{\mathrm{f},m}$ are the macroscopic and microscopic fission cross sections for nuclide m, respectively. $N_m(r)$ is the atomic density for nuclide m at position r. $\chi_{\mathrm{p},m}^{\gamma}$ is prompt photon spectra for fissionable nuclide m. $\nu_{\mathrm{p},m}^{\gamma}$ is the prompt photon yield per fission for fissionable nuclide m. $\Sigma_{\gamma,m'}$ and $\sigma_{\gamma,m}$ are the macroscopic and microscopic capture cross sections for nuclide m', respectively. $N_{m'}(r)$ is the atomic density for nuclide m' at position r. $\chi_{\mathrm{d},m''}^{\mathrm{n}}$ is the delayed photon spectra for nuclide m''. $\lambda_{\mathrm{d},m''}^{\gamma}$ is the delay constant for nuclide m''. $N_{m''}(r)$ is the atomic density for nuclide m'' at position r. $\Sigma_{\gamma\mathrm{n}}$ and $\sigma_{\gamma\mathrm{n}}$ are the macroscopic and microscopic Be(γ, n) cross section. $N_{\mathrm{Be}}(r)$ is the atomic density for nuclide Be at position r. μ_{c} is the Compton effect which alters the direction and energy of the incident photons. μ represents the removal of photons due to the photoelectric reactions and pair productions.

The neutron sources ($\mathbf{S}^{\mathrm{n}}$) can be written as

$$\mathbf{S}^{\mathrm{n}} = (\mathbf{F}_{\mathrm{p}}^{\mathrm{n}} + \mathbf{D}_{\mathrm{d}}^{\mathrm{n}})\phi + \mathbf{H}^{\mathrm{ph}}\psi. \tag{5}$$

From the perturbation theory, the effective delayed neutron fraction is defined as

$$\beta_{\mathrm{eff}} \equiv \frac{\langle \phi^{+}\mathbf{S}_{\mathrm{d}}^{\mathrm{n}} \rangle}{\langle \phi^{+}\mathbf{S}^{\mathrm{n}} \rangle}, \tag{6}$$

where the symbol <···> denotes integration over the full phase space, φ^{+} is the adjoint neutron flux, $\mathbf{S}_{\mathrm{d}}^{\mathrm{n}}$ is the delayed term in the neutron source ($\mathbf{S}^{\mathrm{n}}$) which includes the conventional delayed fission term ($\mathbf{D}_{\mathrm{d}}^{\mathrm{n}}\varphi$) and the delayed photoneutron term ($\mathbf{H}_{\mathrm{d}}^{\mathrm{ph}}\psi$) in this case. The total effective delayed neutron fraction ($\beta_{\mathrm{eff}}^{\mathrm{total}}$) can be expressed as

$$\beta_{\mathrm{eff}}^{\mathrm{total}} = \beta_{\mathrm{eff}}^{\mathrm{n}} + \beta_{\mathrm{eff}}^{\mathrm{ph}} = \frac{\langle \phi^{+}\mathbf{D}_{\mathrm{d}}^{\mathrm{n}}\phi \rangle}{\langle \phi^{+}\mathbf{S}^{\mathrm{n}} \rangle} + \frac{\langle \phi^{+}\mathbf{H}_{\mathrm{d}}^{\mathrm{ph}}\psi \rangle}{\langle \phi^{+}\mathbf{S}^{\mathrm{n}} \rangle}. \tag{7}$$

The first term, $\beta_{\mathrm{eff}}^{\mathrm{n}}$, is the fraction of effective delayed neutrons generated by the fission products. The second term, $\beta_{\mathrm{eff}}^{\mathrm{ph}}$, is the fraction of effective neutrons created by the delayed photons. In Ref. [16], $\beta_{\mathrm{eff}}^{\mathrm{ph}}$ is represented as the sum of the fraction of effective neutrons created by the prompt photons ($\beta_{\mathrm{eff}}^{\mathrm{ph,p}}$) and the fraction of effective neutrons created by the delayed photons ($\beta_{\mathrm{eff}}^{\mathrm{ph,d}}$), i.e., $\beta_{\mathrm{eff}}^{\mathrm{ph}} = \beta_{\mathrm{eff}}^{\mathrm{ph,d}} + \beta_{\mathrm{eff}}^{\mathrm{ph,p}}$. In this paper, $\beta_{\mathrm{eff}}^{\mathrm{ph,p}}$ is removed from $\beta_{\mathrm{eff}}^{\mathrm{ph}}$. The prompt photons are generated within 10^{-11} s after the fission event and the photons are transported "instantaneously," as the photon speed is much greater than the neutron speed.

Since the delayed fission neutrons are generated from a few milliseconds to a few minutes after the fission event, the photoneutrons from the prompt photons are excluded from the delayed neutron source. Dionne and Hanan [16] evaluated $\beta_{\mathrm{eff}}^{\mathrm{ph,d}}$ without considering the delayed photons in the calculation code. The upper limit of $\beta_{\mathrm{eff}}^{\mathrm{ph,d}}$ was represented by twice as $\beta_{\mathrm{eff}}^{\mathrm{ph,p}}$ and the lower limit was zero, as the total energy produced per fission for the delayed photons was slightly smaller than the prompt ones. In this paper, $\beta_{\mathrm{eff}}^{\mathrm{ph}}$ is still evaluated by $\beta_{\mathrm{eff}}^{\mathrm{ph,p}}$, i.e., $\beta_{\mathrm{eff}}^{\mathrm{ph}} = \beta_{\mathrm{eff}}^{\mathrm{ph,d}} = \beta_{\mathrm{eff}}^{\mathrm{ph,p}}$ based on the approximation that the prompt photons provide about the same photoneutron production rate as the delayed photons in reactor with the precursors in equilibrium. For ^{235}U, the average yields of the prompt and delayed photons per fission are 7.2727 and 6.7273, respectively [14, 15]. The average energies of the prompt and delayed photons are 6.61 and 6.11 MeV, respectively.

Table 2 Notations of the operators in Eqs. (2–6)

Operator	Neutron	Photon
Prompt source	$\mathbf{F}_{\mathrm{p}}^{\mathrm{n}}\phi \equiv \sum_m \chi_{\mathrm{p},m}^{\mathrm{n}} \iint \nu_{\mathrm{p},m}^{\mathrm{n}} \Sigma_{\mathrm{f},m}(r,E')\phi(r,t,\mathbf{\Omega}',E')\mathrm{d}E'\mathrm{d}\mathbf{\Omega}'$ $\Sigma_{\mathrm{f},m}(r,E') = \sigma_{\mathrm{f},m}(E')N_m(r)$	$\mathbf{F}_{\mathrm{p}}^{\gamma}\phi \equiv \sum_m \chi_{\mathrm{p},m}^{\gamma} \iint \nu_{\mathrm{p},m}^{\gamma} \Sigma_{\mathrm{f},m}(r,E')\phi(r,t,\mathbf{\Omega}',E')\mathrm{d}E'\mathrm{d}\mathbf{\Omega}'$ $+\sum_{m'} \iint \Sigma_{\gamma,m'}(r,E')\phi(r,t,\mathbf{\Omega}',E')\mathrm{d}E'\mathrm{d}\mathbf{\Omega}'$ $\Sigma_{\gamma,m'}(r,E') = \sigma_{\gamma,m'}(E')N_{m'}(r)$
Delayed source	$\mathbf{D}_{\mathrm{d}}^{\mathrm{n}}\phi \equiv \sum_m \chi_{\mathrm{d},m}^{\mathrm{n}} \iint \nu_{\mathrm{d},m}^{\mathrm{n}} \Sigma_{\mathrm{f},m}(r,E')\phi(r,t,\mathbf{\Omega}',E')\mathrm{d}E'\mathrm{d}\mathbf{\Omega}'$	$\mathbf{D}_{\mathrm{d}}^{\gamma}\phi \equiv \sum_{m''} \chi_{\mathrm{d},m''}^{\gamma} \lambda_{\mathrm{d},m''}^{\gamma} N_{m''}(r)$
Removal	$\mathbf{M}^{\mathrm{n}}\phi \equiv \mathbf{\Omega}\cdot\nabla\phi + \Sigma_t\phi$ $-\iint \Sigma_{\mathrm{s}}(r,E' \to E,\mathbf{\Omega}' \to \mathbf{\Omega})\phi(r,t,\mathbf{\Omega}',E')\mathrm{d}E'\mathrm{d}\mathbf{\Omega}'$	$\mathbf{M}^{\gamma}\psi \equiv \mathbf{\Omega}\cdot\nabla\psi + \mu\psi$ $-\iint \mu_{\mathrm{c}}(r,E' \to E,\mathbf{\Omega}' \to \mathbf{\Omega})\psi(r,t,\mathbf{\Omega}',E')\mathrm{d}E'\mathrm{d}\mathbf{\Omega}'$
Photoneutron source	$H^{\mathrm{ph}}\psi \equiv \chi^{\gamma\mathrm{n}}(E)\iint \Sigma_{\gamma\mathrm{n}}(r,E',\mathbf{\Omega}')\psi(r,t,\mathbf{\Omega}',E')\mathrm{d}E'\mathrm{d}\mathbf{\Omega}';\ \Sigma_{\gamma\mathrm{n}}(r,E') = \sigma_{\gamma\mathrm{n}}(E')N_{\mathrm{Be}}(r)$	

The approximation has been verified in BCNT, which is a reactor using beryllium reflector [25].

3.2 The *k*-ratio method

In 1997, Bretscher [17] introduced the *k*-ratio method for a system without photoneutrons. With some approximations, the effective delayed fission neutron fraction can be evaluated by the ratio between the total and the prompt multiplication factors. This is the reason why this method is called the *k*-ratio method. It has been widely used worldwide [18–21].

For the system with photoneutrons, one can still obtain the exact definition of the delayed fission neutron fraction based on the fact that the photoneutron term is several orders of magnitude smaller than the fission neutron term. Hence, the effective delayed fission neutron fraction ($\beta_{\mathrm{eff}}^{\mathrm{n}}$) can be obtained by MCNP6 [22] calculation with and without delayed neutrons (TOTNU card) while omitting the photoneutrons, which leads to Eq. (9), where the superscript N denotes "MODE N" calculation in MCNP6 and the subscript p represents that generation of the delayed neutron is suppressed.

$$\beta_{\mathrm{eff}}^{\mathrm{n}} \approx 1 - \frac{k_{\mathrm{p}}^{\mathrm{N}}}{k^{\mathrm{N}}}. \tag{9}$$

The *k*-ratio method has been extended to calculate the effective photoneutron fraction (β^{ph}) [16], which can be performed by coupled neutron–photon transport (MODE N P). (γ, n) reactions are modeled with MPN card. It is worth mentioning that $\beta_{\mathrm{eff}}^{\mathrm{ph}}$ is evaluated by $\beta_{\mathrm{eff}}^{\mathrm{ph,p}}$ in this paper, which can be estimated by Eq. (10), where the superscript "N + P" denotes "MODE N P" calculation in MCNP6.

$$\beta_{\mathrm{eff}}^{\mathrm{ph}} = \beta_{\mathrm{eff}}^{\mathrm{total}} - \beta_{\mathrm{eff}}^{\mathrm{n}} = \frac{k^{\mathrm{N+P}} - k_{\mathrm{p}}^{\mathrm{N}}}{k^{\mathrm{N+P}}} - \frac{k^{\mathrm{N}} - k_{\mathrm{p}}^{\mathrm{N}}}{k^{\mathrm{N}}}. \tag{10}$$

3.3 The inner product method

With the same assumptions, the definition of $\beta_{\mathrm{eff}}^{\mathrm{ph}}$ can be rewritten as Eq. (11) after spatial and energy discretization,

$$\beta_{\mathrm{eff}}^{\mathrm{ph}} = \frac{\left\langle \phi^{+}\mathbf{H}_{\mathrm{d}}^{\mathrm{ph}} \right\rangle}{\left\langle \phi^{+}S^{\mathrm{n}} \right\rangle} = \frac{\sum_I \sum_{\mathrm{n}} \varphi_{\mathrm{n},I}^{+} \sum_{\mathrm{g}'} V_I \Sigma_{\gamma\mathrm{n},\mathrm{g}',I}\psi_{\mathrm{g}',I}}{\sum_I \sum_{\mathrm{n}} \varphi_{\mathrm{n},I}^{+}\chi_{\mathrm{n},I} \sum_{\mathrm{n}'} V_I \upsilon\Sigma_{f,\mathrm{n}',I}\varphi_{\mathrm{n}',I}}, \tag{11}$$

where the generation process of the photons is omitted and the photon flux Ψ is used; $\Sigma_{\gamma,\mathrm{n}}$ represents the (γ, n) reaction; V_I is the volume of cell; the index I refers to the volume cell of the spatial mesh; the indexes n and g refer to the neutron and photon energy group, respectively.

The deterministic and Monte Carlo codes were used together for the effective delayed photoneutron fraction calculations [25], the flow chart of which is shown in Fig. 2. The solution of the adjoint neutron transport equation was unavailable because of the continuous-energy treatment of nuclear data in Monte Carlo Code [18]. The adjoint neutron flux could be obtained through the adjoint diffusion calculation of CITATION [23]. The multi-group constants were calculated by the lattice code PIJ [24]. With the cutoff energy at 1.855 eV, four group (3 fast and 1 thermal groups; Table 3) constants were generated for the CITATION diffusion calculation based on *R*–θ–*Z* geometry.

3.4 Codes and nuclear data libraries

TMSR-SF1 uses coated particle fuels, so the double heterogeneity, caused by the distribution of TRISO fuel particles in the pebbles and the pebble distribution in the core, must be modeled correctly. The general-purpose continuous-energy Monte Caro code MCNP6 version 1.0 was used for explicitly representing the geometry of both fuel pebbles and the individual particle kernels to account for the double heterogeneity effect. It is worth mentioning that all MCNP6 calculations presented in this work were performed with ENDF/B-VII.0 cross sections. The deterministic codes including PIJ and CITATION were used for the forward and adjoint neutron flux calculations. The collision probability method code (PIJ) was used to solve the energy- and space-dependent Boltzmann neutron transport equation numerically by the collision probability

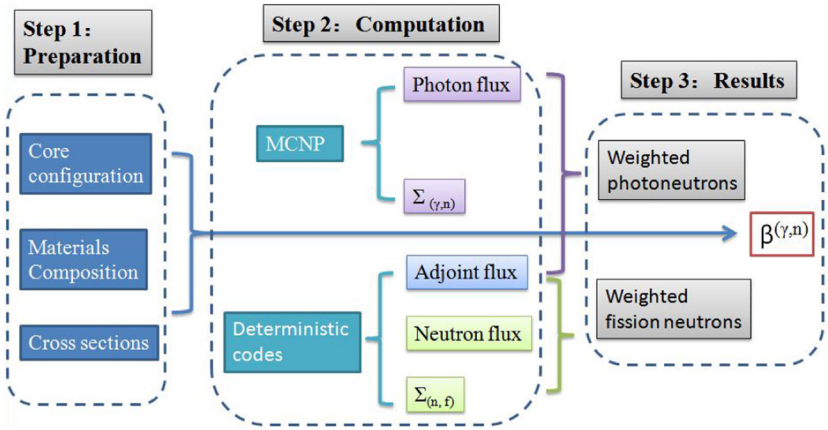

Fig. 2 (Color online) Calculation flow chart

Table 3 Group structure in CITATION calculations

Groups	Energy boundaries	Comment
1	10 MeV–749 keV	Fast, the prompt fission neutron
2	749 keV–18 keV	Fast, the delayed fission neutron
3	18 keV–1.855 eV	Fast
4	1.855 eV–0 eV	Thermal

method. This method has been widely used for treating the double heterogeneity energy self-shielding effect of the pebble bed reactor [1]. At every level of heterogeneity, an artificial material is generated to give transmission probability of the aggregate of each level's constituents. The homogenized material replaces the heterogeneous geometry on the next level of heterogeneity from fine to coarse geometric detail. CITATION, the multi-group diffusion code, was used for three-dimensional core calculation using explicit description of space. Table 4 gives a summary of the codes used in this work.

4 Results

MCNP6 kept high geometric fidelity on the assumption that the pebbles were regularly distributed in the core and the coated particles were regularly distributed in the fuel zone. Meanwhile, a four energy group and $64(\theta) \times$

Table 4 Summary of codes used in this work

Items	Deterministic codes		Monte Carlo
	Fuel cell code	Core calculation code	
Code	PIJ	CITATION	MCNP6 1.0
Theory	Collision probability	Multi-dimensional diffusion	Monte Carlo
Model	Ball	3-D (R–θ–Z)	3-D
Nuclear data	JENDL-3.3	–	ENDF/B-VII.0
Number of groups	107 (cutoff energy 1.86 eV)	3 + 1(fast + thermal)	Continuous

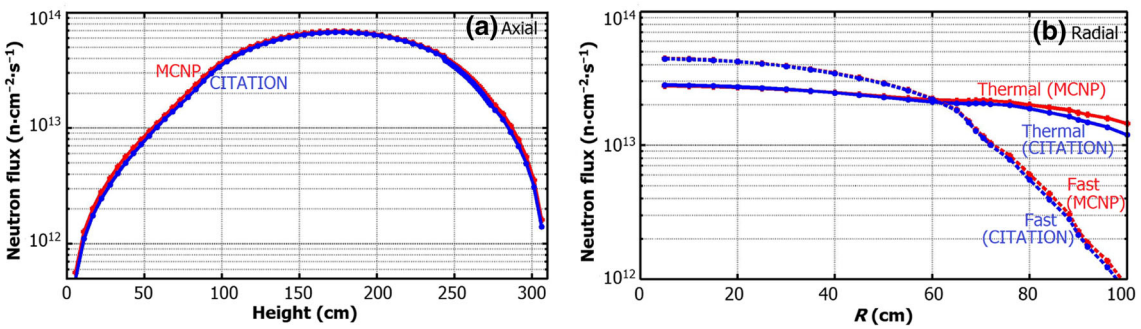

Fig. 3 Axial (**a**) and radial (**b**) neutron flux distribution calculated by MCNP6 and CITATION

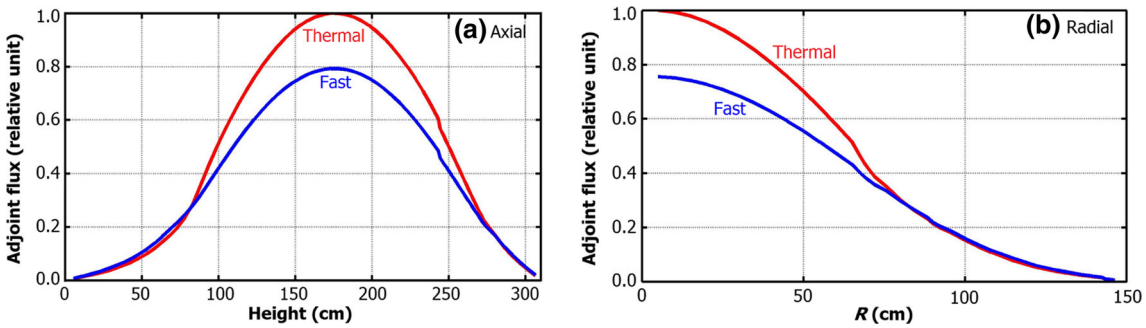

Fig. 4 (Color online) Axial (**a**) and radial (**b**) adjoint neutron flux distribution calculated by CITATION

Table 5 Effective delayed neutron fraction (in pcm) calculated by the *k*-ratio method for TMSR-SF1

Mode N		Mode N, P
k^{N}	$k_{\mathrm{P}}^{\mathrm{N}}$	$k_{\mathrm{P}}^{\mathrm{N+P}}$
0.98708 ± 0.00001	0.98040 ± 0.00001	0.98712 ± 0.00001
$\beta_{\mathrm{eff}}^{\mathrm{n}} = 677 \pm 1.4$		$\beta_{\mathrm{eff}}^{\mathrm{ph}} = 4.0 \pm 1.4$

$34(R) \times 85(Z)$ spatial meshes were modeled by CITATION for TMSR-SF1.

4.1 Neutron flux and adjoint neutron flux

To validate results calculated by CITATION, the neutron flux integrated over energy space calculated by MCNP6 and CITATION was compared. The axial neutron flux in given Z meshes was averaged over θ and R directions, and the radial neutron flux in given R meshes was averaged over θ and Z directions. The axial and radial neutron flux distributions are shown in Fig. 3. The neutron flux distributions calculated by the two codes agree well, except the flux in the reflector zone.

The normalized axial and radial adjoint neutron fluxes calculated by CITATION are shown in Fig. 4. The adjoint neutron fluxes were integrated over energy space at the cutoff energy of 1.86 eV. The axial adjoint neutron flux in given Z meshes was averaged over θ and R directions, and the radial adjoint neutron flux in given R meshes was averaged over θ and Z directions. It can be seen that the thermal neutron had higher weight than the fast neutron in the active zone. The adjoint neutron flux decreased rapidly in the reflector zone as expected, indicating that neutrons in the reflector zone were of much lower importance than the neutrons in the active zone.

4.2 The delayed photoneutron fraction

4.2.1 The k-ratio method

Using the *k*-ratio method, the delayed fission neutron and photoneutron fraction of TMSR-SF1 were calculated with MCNP6. As Be(γ, n) reaction rate is small, 10^{10} neutron histories were performed. The results are given Table 5. The critical eigenvalues were obtained with a standard deviation (1σ) of about 0.00001. The *k*-ratio method, which is based on calculating the multiplication factor with and without the contribution of the photoneutrons and delayed fission neutrons, is time-consuming. Also, it introduces relatively large statistical errors for the effective delayed photoneutrons fraction.

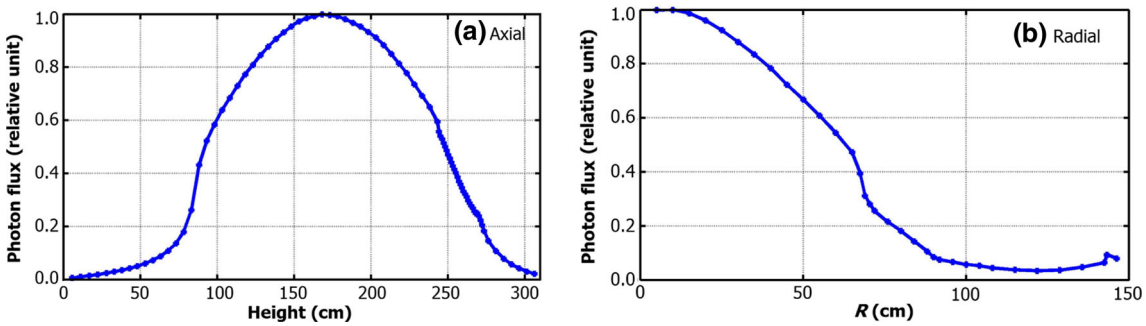

Fig. 5 (Color online) Axial (**a**) and radial (**b**) photon flux distribution calculated by MCNP6

Table 6 Effective photoneutron fraction calculated by the inner product method

Weighted fission neutrons in the active zone		4.44E−15 (±2.70E−20)
Weighted photoneutrons in the core		1.43E−19 (±3.62E−22)
$\beta_{\text{eff}}^{\text{ph}}$ (pcm)		3.22 (±0.01)
Regions with coolant	Coolant volume (m^3)	Contribution for $\beta_{\text{eff}}^{\text{ph}}$
Active zone with fuel pebbles	0.99	96.65%
Top and bottom reflector zone	0.50	1.26%
Side reflector zone	1.20	2.09%

4.2.2 The inner product method

With the same meshes, the axial and radial distributions of photon flux integrated over the energy space were calculated by MCNP6. As shown in Fig. 5a, the photon flux decreased quickly from the core center to the edges. It can be deduced that photons are mostly generated in the process of fission. In Fig. 5b, there is a small peak at about 140 cm. The main reason is neutron absorption in Hastelloy N alloy vessel.

The calculated photoneutron fraction combining MCNP6 and CITATION is listed in Table 6, based on the methodology explained in Sect. 3. It is worth mentioning that the photon fluxes are calculated by MCNP6, so there are statistical uncertainties. It is found that the weighted photoneutrons generated in the active zone take majority share, about 96.65%, while the ones outside the active region account for only 3.35%. This coincides with the photon flux distribution.

5 Conclusion

The *k*-ratio and the inner product methods were used to estimate the effective delayed photoneutron fraction in TMSR-SF1. The Monte Carlo code MCNP6 was used to calculate the photoneutron fraction using the *k*-ratio method. The inner product methods were performed by Monte Carlo code and deterministic codes together. The neutron flux calculation of CITATION was validated by Monte Carlo code. It is shown that the neutron flux distributions performed by the Monte Carlo code and deterministic codes agree with each other in general. The effective delayed photoneutron fraction calculated by the *k*-ratio method is about 4.0 pcm (±1.4 pcm). The result calculated by the inner product method is 3.22 pcm (± 0.01 pcm). The results show that there are good agreements between two methods.

Influence of the effective delayed photoneutron fraction on the dynamic characteristics will be analyzed for TMSR-SF1.

References

1. T. Allen, S. Ball, E Blandford et al., in *Preliminary fluoride salt-cooled high temperature reactor (FHR) subsystems definition, functional requirement definition and licensing basis event (LBE) identification white paper*. University of California, Berkeley, UCBTH-12-001 (2012)
2. C. Forsberg, L.W. Hu, J. Richard et al., in *Fluoride-salt-cooled high temperature test reactor (FHTR): goals, options, ownership, requirements, design, licensing, and support facilities*. Massachusetts Institute of Technology, MIT-ANP-TR-154 (2014)
3. K. Sun, L.W. Hu, C. Forsberg, Neutronic design features of a transportable fluoride-salt-cooled high-temperature reactor. ASME J. Nucl. Radiat. Sci. **2**, 031003-031003-10 (2016). doi:10.1115/1.4032873
4. M.H. Jiang, H.J. Xu, Z.M. Dai, Advanced fission energy program—TMSR nuclear energy system. Bull. Chin. Acad. Sci. **27**, 366–374 (2012). doi:10.3969/j.issn.1000-3045.2012.03.016
5. TMSR group, in *TMSR-SF1 conceptual design overview, chapter 2*. Shanghai Institute of Applied Physics, Shanghai (2015)
6. M. Aufiero, M. Fratoni, in *Development of multi-physics tools for fluoride-cooled high-temperature reactors*. PHYSOR 2016, Sun Valley, 1–5 May 2016
7. C.E. Cohn, Errors in reactivity measurements due to photoneutrons effects. Nucl. Sci. Eng. **6**, 284–287 (1959)
8. G. Hordósy, A. Keresztúri, P. Vértes et al., Influence of the photoneutrons on the kinetics of the beryllium reflected core of the budapest research reactor. In *Advanced Monte Carlo for Radiation Physics, Particle Transport Simulation and Applications*, Lisbon, 23–26 Oct 2000
9. S.S. Lomakin, YuA Nechaev, Transient processes and the measurement of reactivity of a reactor containing beryllium. Sov. At. Energy **18**, 35–42 (1965). doi:10.1007/BF01116353
10. F.B. Buoni, in *Experience with the use of the rod-drop method of rod calibration at the ORR and LITR*. ORNL, ORNL-TM-605 (1963)
11. L.J. Meng, W. Lai, G.Q. Huang et al., Design and verification of a portable reactivity meter used for high temperature reactor. Nucl. Electron. Detect. Technol. **35**, 917–920 (2015). doi:10.3969/j.issn.0258-0934.2015.09.017. **(in Chinese)**
12. R.M. Ji, M.H. Li, Y. Zou et al., Impact of photoneutrons on reactivity measurements for TMSR-SF1. Nucl. Sci. Tech. **28**, 76 (2017). doi:10.1007/s41365-017-0234-7
13. M. Carta, S. Dulla, V. Peluso et al., Calculation of the effective delayed neutron fraction by deterministic and monte carlo methods. Sci. Technol. Nucl. Install. (2011). doi:10.1155/2011/584256. **(Article ID 584256)**
14. F. Jatuff, A. Lüthi, M. Murphy et al., Measurement and interpretation of delayed photoneutrons effects in multizone criticals with partial D_2O moderation. Ann. Nucl. Energy **30**, 1731–1755 (2003). doi:10.1016/S0306-4549(03)00136-1

15. M.S. Onegin, Delayed photoneutrons in the PIK reactor. At. Energy **107**, 194–201 (2009). doi:10.1007/s10512-010-9215-1
16. B. Dionne, N. Hanan, Impact of photoneutrons on transients for the MURR and MITR HEU and LEU cores. In *The 32nd RERTR 2010 International Meeting on Reduced Enrichment for Research and Test Reactors*, Lisbon, 10–14 Oct 2010
17. M.M. Bretscher, Perturbation independent methods for calculating research reactor kinetic parameters, Argonne National Laboratory, ANL/RERTR/TM30 (1997)
18. Z. Zhong, A. Talamo, Y. Gohar, Monte Carlo and deterministic computational methods for the calculation of the effective delayed neutron fraction. Comput. Phys. Commun. **184**, 1660–1665 (2013). doi:10.1016/j.cpc.2013.02.009
19. V. Bécares, S. Pérez-Martín, M. Vázquez-Antolín et al., Review and comparison of effective delayed neutron fraction calculation methods with Monte Carlo codes. Ann. Nucl. Energy **65**, 402–410 (2014). doi:10.1016/j.anucene.2013.11.038
20. M. Arkani, M. Hassanzadeh, S. Khakshournia, Calculation of six-group importance weighted delayed neutron fractions and prompt neutron lifetime of MTR research reactors based on Monte Carlo method. Prog. Nucl. Energy **88**, 352–363 (2016). doi:10.1016/j.pnucene.2015.12.005
21. S.A. Hosseinia, M. Athari Allafb, Benchmarking of the HTR-10 reactor's kinetic parameters: effective delayed neutron fraction. Prog. Nucl. Energy **75**, 80–91 (2014). doi:10.1016/j.pnucene.2014.04.015
22. D. B. Pelowitz (ed.), MCNP6™ User's Manual, Los Alamos National Laboratory, LA-CP-13-00634 (2013)
23. T.B. Fowler, D.R. Vondy, G.W. Cummingham, Nuclear reactor analysis code: CITATION. ORNL, USA, ORNL-TM-2496 (1969)
24. K. Tsuchihashi, H. Takano, K. Horikami et al., SRAC2006: a comprehensive neutronics calculation code system. JAEA, Japan, JAEA-Data/Code 2007-004 (2007)
25. F. Shen, Z. Lu, Z.Y. Sun et al., Delayed photon-induced neutron parameters on reactor of in-hospital neutron irradiator for boron neutron capture therapy. At. Energy Sci. Technol. **42**, 697–701 (2008). **(in Chinese)**